



HAL
open science

Online deconvolution for pushbroom hyperspectral imaging systems

Yingying Song, El-Hadi Djermoune, Jie Chen, Cédric Richard, David Brie

► **To cite this version:**

Yingying Song, El-Hadi Djermoune, Jie Chen, Cédric Richard, David Brie. Online deconvolution for pushbroom hyperspectral imaging systems. 2017. hal-01493901v1

HAL Id: hal-01493901

<https://hal.science/hal-01493901v1>

Preprint submitted on 22 Mar 2017 (v1), last revised 5 Feb 2018 (v2)

HAL is a multi-disciplinary open access archive for the deposit and dissemination of scientific research documents, whether they are published or not. The documents may come from teaching and research institutions in France or abroad, or from public or private research centers.

L'archive ouverte pluridisciplinaire **HAL**, est destinée au dépôt et à la diffusion de documents scientifiques de niveau recherche, publiés ou non, émanant des établissements d'enseignement et de recherche français ou étrangers, des laboratoires publics ou privés.

ONLINE DECONVOLUTION FOR PUSHBROOM HYPERSPECTRAL IMAGING SYSTEMS

Yingying Song¹, El-Hadi Djermoune¹, Jie Chen², Cédric Richard³ and David Brie¹

¹CRAN, Université de Lorraine, CNRS, Vandœuvre-lès-Nancy, France

²Northwestern Polytechnical University, Xi'an, China

³Université Côte d'Azur, CNRS, OCA, Nice, France

ABSTRACT

This paper introduces a framework based on the LMS algorithm for sequential deconvolution of hyperspectral images acquired by pushbroom imaging systems. Considering a sequential model of image blurring phenomenon, we derive a sliding-block regularized LMS algorithm with spatial and spectral regularizers. The performance of the algorithm is evaluated using real hyperspectral data. The role of the hyperparameters is also discussed.

Index Terms— Hyperspectral image, online deconvolution, LMS

1. INTRODUCTION

Hyperspectral imaging has received considerable attention in the last decade as it combines the power of digital imaging and spectroscopy. Every pixel in a hyperspectral image provides local spectral information about a scene of interest across a large number of contiguous bands. This information can be used to characterize objects with great precision and detail in a number of areas, including agricultural monitoring, industrial inspection, and defense. The core characteristics of hyperspectral images raise new data processing issues ranging from image restoration to pattern recognition [1, 2].

Several sensing techniques have been developed for hyperspectral imaging. They can be categorized into four main groups [3, 4]: whiskbroom (point scan), pushbroom (line scan), tunable filter (wavelength scan), and snapshot. Figure 1 depicts schematically how a hyperspectral image is captured by a pushbroom imager, and how the spatial-spectral arrays are stacked within a hyperspectral image datacube. With the pushbroom technique, pixel spectra are sensed line-by-line at each time instant. The scene is typically scanned by moving the imager or its field of view across the scene. Pushbroom systems are used in many areas such as food safety [5,6], georeferencing [7] and material sorting [8,9].

The aim of this paper is to address the problem of online (sequential) deconvolution of hyperspectral images pro-

vided by pushbroom imaging systems such as those described in [3, 10]. Image deconvolution deals with restoring an original image from blurred and, generally, noisy observations. Multichannel images restoration was carried out with Wiener methods in [11, 12]. Other strategies such as [13–16] were also introduced, but only in an offline setting.

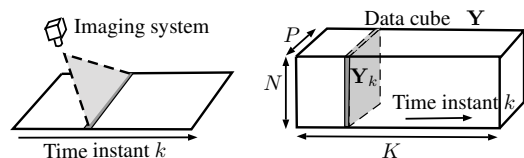


Fig. 1: Data acquisition by a pushbroom imaging system

Consider a hyperspectral image $\mathbf{Y} \in \mathbb{R}^{N \times P \times K}$ collected by a pushbroom hyperspectral imaging system, where N , P , and K denote the number of spatial, spectral, and time measurements, respectively. The samples to be imaged are carried by a conveyor moving at constant speed. The hyperspectral image is then acquired slice by slice, each of which is denoted by $\mathbf{Y}_k \in \mathbb{R}^{N \times P}$. The size of \mathbf{Y} increases with k which can possibly grow to infinity. The acquisition parameters are the spatial sampling Δ and integration time T . We consider situations where the spatial sampling Δ is smaller than the support of the point spread function, which results in a spatial blurring of the hyperspectral image, and the integration time is small (for fast scanning) yielding a low signal to noise ratio. This motivates the derivation of sequential deconvolution algorithms that are able to restore, in an online way, an hyperspectral image \mathbf{X} from a noisy and blurred observation \mathbf{Y} . The main contribution of this work is to introduce an LMS framework for sequential deconvolution of hyperspectral images. While our algorithm operates in the spirit of LMS-based algorithms used, for instance, for adaptive system identification [17–19] and adaptive superresolution image restoration [20,21], sequential image deconvolution of hyperspectral images based on the LMS has never been reported in the literature. Accounting for the specificity of the acquisition process, we propose a sliding-block LMS algorithm that allows to sequentially restore the hyperspectral image of interest with

This work has been supported by the FUI AAP 2015 Trispirabois Project, the Conseil Régional de Lorraine and the GDR ISIS.

a delay Q . We also introduce regularization terms promoting the restoration of piecewise constant objects on a background which should be zero-valued.

2. BLURRING AND CAUSALITY ISSUES

We shall now discuss issues related to the causality of convolution kernel and associated estimates. Following [15], hyperspectral image blurring can be seen as P simultaneous spatial convolutions. For each wavelength λ_p , the blurred spatial image $\mathbf{Y}^p \in \mathbb{R}^{N \times K}$ is given by the 2D convolution:

$$\mathbf{Y}^p = \bar{\mathbf{H}}^p * \mathbf{X}^p + \mathbf{Z}^p \quad (1)$$

where $*$ is the 2D convolution operator, $\mathbf{X}^p \in \mathbb{R}^{N \times K}$ is the image to restore, $\bar{\mathbf{H}}^p \in \mathbb{R}^{M \times L}$ is a convolution kernel (filter), and \mathbf{Z}^p is a noise supposed to be additive and i.i.d. We first derive a sequential causal formulation of model (1). Without loss of generality, we shall focus on the sequential model for 2D images, by omitting the dependence with respect to p . The image \mathbf{Y} , collected in an online way, can be represented as a sequence of vectors $\mathbf{y}_k := [y_{1,k}, \dots, y_{N,k}]^\top$, $k = 1, \dots, K$, where \top denotes the transpose of a matrix. We shall use the same notation for \mathbf{X} . We assume a finite length blurring kernel of size L along the time dimension, centered around 0 which means that past and future values of \mathbf{x}_k contribute to the observation \mathbf{y}_k . In order to make the blurring kernel causal¹, it has to be shifted by $(L-1)/2$, which means that the observations needs to be delayed by $(L-1)/2$ samples, that is, $\tilde{\mathbf{y}}_k = \mathbf{y}_{k-(L-1)/2}$. Writing $\bar{\mathbf{H}} = [\mathbf{h}_L, \dots, \mathbf{h}_1]$ with $\mathbf{h}_\ell = [h_{M,\ell}, \dots, h_{1,\ell}]^\top$, model (1) can be expressed as:

$$\tilde{\mathbf{y}}_k = \mathbf{y}_{k-(L-1)/2} = \sum_{\ell=1}^L \mathbf{H}_\ell \mathbf{x}_{k-\ell+1} + \mathbf{z}_k \quad (2)$$

where \mathbf{z}_k is a zero-mean measurement noise, statistically independent of the other signals. \mathbf{H}_ℓ is the $N \times N$ Toeplitz matrix with first column and first row given by $[h_{1,\ell}, \dots, h_{M,\ell}, 0, \dots, 0]$ and $[h_{1,\ell}, 0, \dots, 0]$, respectively. Relation (2) introduces a delay in both time dimension and spatial dimension because the filter is made causal along these two dimensions. Another consequence of causality issues concerns the estimation process of \mathbf{x}_k . First, \mathbf{x}_k is involved in past and future observations ($\mathbf{y}_{k-(L-1)/2}, \dots, \mathbf{y}_k, \dots, \mathbf{y}_{k+(L-1)/2}$). Secondly, optimally estimating \mathbf{x}_k requires all the past and future estimations ($\dots, \hat{\mathbf{x}}_{k-2}, \hat{\mathbf{x}}_{k-1}, \hat{\mathbf{x}}_{k+1}, \hat{\mathbf{x}}_{k+2}, \dots$), which precludes the estimation of \mathbf{x}_k in a sequential manner. To address these issues, we recommend to produce the estimates $\hat{\mathbf{x}}_k$ with a delay Q . This means that we shall estimate \mathbf{x}_{k-Q+1} given ($\mathbf{y}_{k+(L-1)/2-Q+1}, \dots, \mathbf{y}_{k+(L-1)/2}$), coarse posterior estimates ($\hat{\mathbf{x}}_k, \hat{\mathbf{x}}_{k-1}, \dots, \hat{\mathbf{x}}_{k-Q+2}$) refined as k increases, and past estimates ($\hat{\mathbf{x}}_{k-Q}, \hat{\mathbf{x}}_{k-Q-1}, \dots, \hat{\mathbf{x}}_{k-Q-L+2}$). This is the

¹For simplicity, L is assumed to be odd.

key idea of the sliding-block LMS deconvolution algorithm developed in the next section.

3. ONLINE IMAGE DECONVOLUTION

We shall first address the adaptive deconvolution problem in the case of 2D images. Then the proposed algorithm will be extended to hyperspectral images. Consider the problem of estimating \mathbf{x}_{k-Q+1} in a sequential manner based on observations ($\mathbf{y}_{k+(L-1)/2-Q+1}, \dots, \mathbf{y}_{k+(L-1)/2}$) or, equivalently, on the delayed ones ($\tilde{\mathbf{y}}_{k-Q+1}, \dots, \tilde{\mathbf{y}}_k$). In what follows, to simplify notations, \mathbf{y}_k refers to the delayed observation $\tilde{\mathbf{y}}_k$. To account for their dependencies on $\mathbf{x}_k, \dots, \mathbf{x}_{k-Q-L+2}$, we consider the following criterion:

$$\begin{aligned} \mathcal{J}(\mathbf{x}_k, \dots, \mathbf{x}_{k-Q-L+2}) = & \sum_{q=1}^Q \mathbb{E} \left\| \mathbf{y}_{k-q+1} - \sum_{\ell=1}^L \mathbf{H}_\ell \mathbf{x}_{k-q-\ell+2} \right\|^2 \\ & + \eta_s \sum_{q=1}^Q \|\mathbf{D}_N \mathbf{x}_{k-q+1}\|_1 + \eta_t \sum_{q=1}^{Q-1} \|\mathbf{x}_{k-q+1} - \mathbf{x}_{k-q}\|_1 \\ & + \eta_z \sum_{q=1}^Q \|\mathbf{x}_{k-q+1}\|_1 \end{aligned} \quad (3)$$

where $\|\cdot\|_1 = \sum_{n=1}^N |\{\cdot\}_n|$ denotes the ℓ_1 -norm, and $\{\cdot\}_n$ stands for the n -th entry of a vector. Define the first-order derivative filter \mathbf{D}_N as an $(N-1) \times N$ Toeplitz matrix with first column $[1, 0, \dots, 0]$ and first row $[1, -1, 0, \dots, 0]$. The regularizers $\|\mathbf{D}_N \mathbf{x}_{k-q+1}\|_1$ and $\|\mathbf{x}_{k-q+1} - \mathbf{x}_{k-q}\|_1$ promote the restoration of piecewise constant patterns along the spatial and time dimensions, respectively, and the zero-attracting regularizer $\|\mathbf{x}_{k-q+1}\|_1$ promotes the removal of the conveyor background. The choice of these regularization terms is thus motivated by the targeted application, namely, the inspection of objects put on the conveyor belt. At a given wavelength, the response of the conveyor after background removal is close to zero while that of the objects is supposed to be piecewise constant. The strength of the first derivative regularizers along spatial and time dimensions are controlled by $\eta_s \geq 0$ and $\eta_t \geq 0$, respectively. The strength of the zero-attracting regularizer is controlled by $\eta_z \geq 0$.

3.1. Sliding-block regularized LMS (SBR-LMS)

We shall now devise the sliding-block regularized LMS algorithm. Consider vectorized data:

$$\mathbf{x}'_k \triangleq \text{col}\{\mathbf{x}_{k-q+1}\}_{q=1}^{Q+L-1}, \quad \mathbf{y}'_k \triangleq \text{col}\{\mathbf{y}_{k-q+1}\}_{q=1}^{Q+L-1}$$

where $\text{col}\{\cdot\}$ stacks its vector arguments on top of each other. A subgradient of (3) is given by:

$$\nabla \mathcal{J}(\mathbf{x}'_k) \triangleq \begin{bmatrix} \frac{\partial \mathcal{J}}{\partial \mathbf{x}_k} \\ \vdots \\ \frac{\partial \mathcal{J}}{\partial \mathbf{x}_{k-Q-L+2}} \end{bmatrix} = \begin{bmatrix} \frac{\partial \mathcal{J}}{\partial \mathbf{x}_k} \\ \vdots \\ \frac{\partial \mathcal{J}}{\partial \mathbf{x}_{k-Q+1}} \\ \mathbf{0}_{N \times 1} \\ \vdots \\ \mathbf{0}_{N \times 1} \end{bmatrix} \quad (4)$$

where $\mathbf{0}_{I \times J}$ denotes the $I \times J$ zero matrix. Approximating the subgradient in (4) by its instantaneous value yields:

$$\nabla \mathcal{J}(\mathbf{x}'_k) = -2\Phi(\mathbf{y}'_k - \mathbf{G}\mathbf{x}'_k) + \eta_s \mathbf{D}_s^\top \text{sign}(\mathbf{D}_s \mathbf{x}'_k) + \eta_t \mathbf{D}_t^\top \text{sign}(\mathbf{D}_t \mathbf{x}'_k) + \eta_z \text{sign}(\mathbf{x}'_k) \quad (5)$$

where Φ and \mathbf{G} are matrices of size $(Q+L-1)N \times (Q+L-1)N$. Matrix Φ is given by:

$$\Phi \triangleq \begin{bmatrix} \mathbf{H}_1^\top & & \mathbf{0} & \\ \vdots & \ddots & & \\ \mathbf{H}_Q^\top & \dots & \mathbf{H}_1^\top & \\ \hline & \mathbf{0}_{(L-1)N \times QN} & & \mathbf{0}_{(L-1)N \times (L-1)N} \end{bmatrix},$$

with $\mathbf{H}_\ell = \mathbf{0}_{N \times N}$ for $\ell > L$, and \mathbf{G} a block-Toeplitz matrix whose first block column is $[\mathbf{H}_1, \mathbf{0}_{N \times N}, \dots, \mathbf{0}_{N \times N}]$ and first block row is $[\mathbf{H}_1, \dots, \mathbf{H}_L, \mathbf{0}_{N \times N}, \dots, \mathbf{0}_{N \times N}]$. The first-order derivative filters for spatial and time dimensions are:

$$\mathbf{D}_s \triangleq [\mathbf{I}_Q \otimes \mathbf{D}_N \quad \mathbf{0}_{Q(N-1) \times (L-1)N}]$$

$$\mathbf{D}_t \triangleq [\mathbf{D}_Q \otimes \mathbf{I}_N \quad \mathbf{0}_{(Q-1)N \times (L-1)N}],$$

where \otimes stands for the Kronecker product and \mathbf{I}_J denotes the $J \times J$ identity matrix. The sign function is defined as $\text{sign}(x) = 0$ for $x = 0$, and $\text{sign}(x) = x/|x|$ otherwise. Finally, the SBR-LMS algorithm for image deconvolution is given by:

$$\hat{\mathbf{x}}'_{k+1} = \Omega \hat{\mathbf{x}}'_k - \frac{\mu}{2} \nabla \mathcal{J}(\hat{\mathbf{x}}'_k)$$

$$= \Omega \hat{\mathbf{x}}'_k + \mu \Phi(\mathbf{y}'_k - \mathbf{G}\hat{\mathbf{x}}'_k) - \rho_s \mathbf{D}_s^\top \text{sign}(\mathbf{D}_s \hat{\mathbf{x}}'_k) - \rho_t \mathbf{D}_t^\top \text{sign}(\mathbf{D}_t \hat{\mathbf{x}}'_k) - \rho_z \text{sign}(\hat{\mathbf{x}}'_k) \quad (6)$$

where μ is a step size parameter that controls the convergence rate and the algorithm stability, and

$$\Omega \triangleq \begin{bmatrix} \mathbf{I}_{(Q-1)N} & \mathbf{0} & \mathbf{0} & \mathbf{0}_{(Q-1)N \times N} \\ \mathbf{0} & \mathbf{I}_N & \mathbf{0} & \mathbf{0}_{N \times N} \\ \mathbf{0} & \mathbf{0} & \mathbf{I}_N & \mathbf{0}_{N \times N} \\ \mathbf{0} & \mathbf{0} & \mathbf{I}_{(L-2)N} & \mathbf{0}_{(L-2)N \times N} \end{bmatrix},$$

$\rho_s = \mu\eta_s/2$, $\rho_t = \mu\eta_t/2$ and $\rho_z = \mu\eta_z/2$. The final result \mathbf{x}_{k-Q+2} is obtained by selecting the Q -th block of vector $\hat{\mathbf{x}}'_{k+1}$, that is,

$$\hat{\mathbf{x}}_{k-Q+2} = \mathbf{S}\hat{\mathbf{x}}'_{k+1} \quad (7)$$

where $\mathbf{S} \triangleq [\mathbf{0}_{N \times (Q-1)N}, \mathbf{I}_N, \mathbf{0}_{N \times (L-1)N}]$. When $Q = 1$ and $\rho_s = \rho_t = 0$, algorithm (6) reduces to the Zero-Attracting LMS (ZA-LMS) algorithm proposed in [18] for sparse system identification.

3.2. Online hyperspectral image deconvolution

Consider now the problem of 3D hyperspectral image deconvolution, which aims at restoring sequentially spatial-spectral arrays $\mathbf{X}_k \in \mathbb{R}^{N \times P}$. In an equivalent way, we shall consider vectorized data

$$\mathbf{x}'_k \triangleq \text{col}\{\mathbf{x}'_k{}^p\}_{p=1}^P, \quad \mathbf{y}'_k \triangleq \text{col}\{\mathbf{y}'_k{}^p\}_{p=1}^P$$

where superscript p refers to the spectral band. Adding a spectral regularization term to promote spectral smoothness of the image leads to the criterion:

$$\mathcal{C}(\mathbf{x}'_k) = \sum_{p=1}^P \mathcal{J}(\mathbf{x}'_k{}^p) + \eta_\lambda \|\Lambda_\lambda \mathbf{x}'_k\|^2 \quad (8)$$

where $\Lambda_\lambda \triangleq (\text{diag}(c_1, \dots, c_{P-1}) \mathbf{D}_P) \otimes \mathbf{I}_{(Q+L-1)N}$ is a first-order filtering operator along the spectral dimension weighted by the coefficients $\{c_p\}_{p=1}^{P-1}$. The parameter η_λ controls the strength of the spectral smoothness penalty term. Finally, the SBR-LMS algorithm for hyperspectral image deconvolution can be expressed as:

$$\hat{\mathbf{x}}'_{k+1} = \Gamma \hat{\mathbf{x}}'_k - \frac{\mu}{2} \nabla \mathcal{C}(\hat{\mathbf{x}}'_k)$$

$$= \Gamma \hat{\mathbf{x}}'_k + \mu \Psi(\mathbf{y}'_k - \Upsilon \hat{\mathbf{x}}'_k) - \rho_s \Lambda_s^\top \text{sign}(\Lambda_s \hat{\mathbf{x}}'_k) - \rho_t \Lambda_t^\top \text{sign}(\Lambda_t \hat{\mathbf{x}}'_k) - \rho_z \text{sign}(\hat{\mathbf{x}}'_k) - \mu\eta_\lambda \Lambda_\lambda^\top \Lambda_\lambda \hat{\mathbf{x}}'_k \quad (9)$$

with:

$\Gamma \triangleq \mathbf{I}_P \otimes \Omega$, $\Psi \triangleq \text{blkdiag}\{\Phi^p\}_{p=1}^P$ a block-diagonal matrix, $\Upsilon \triangleq \text{blkdiag}\{\mathbf{G}^p\}_{p=1}^P$, $\Lambda_s \triangleq \mathbf{I}_P \otimes \mathbf{D}_s$, and $\Lambda_t \triangleq \mathbf{I}_P \otimes \mathbf{D}_t$.

4. EXPERIMENTAL RESULTS

The experiment described below aims at evaluating the performance of the SBR-LMS algorithm on a real blurred hyperspectral image of size $581 \times 431 \times 16$ with wavelengths varying from 501.1 nm to 868.6 nm with an increment of 24.5 nm. The conveyor background was estimated from data in an area of size 120×120 . It was then subtracted from the real image. Objects on the background were four pieces of wood, a piece of paper-box cover and a piece of metal. The convolution filter was estimated from data to be a Gaussian kernel of size 21×21 . Its full width at half-maximum was set to 10 pixels. To avoid the storage of matrix \mathbf{H}_ℓ , convolution was performed in the frequency domain.

To show the effect of each regularizer, we first present the deconvolution results obtained on a 2D slice of the hyperspectral image corresponding to the first wavelength, namely,

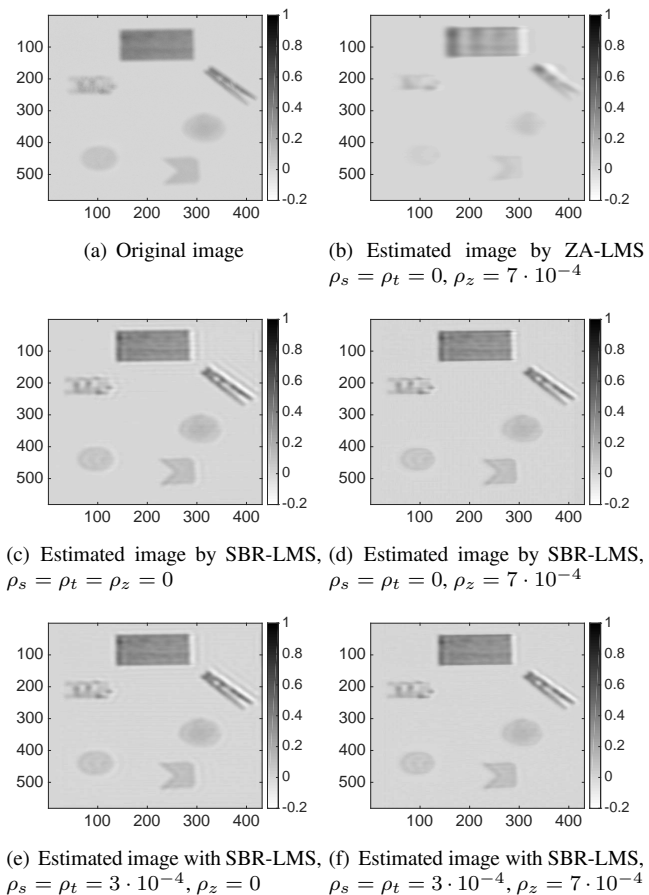


Fig. 2: Comparison of different regularization parameters.

501.1 nm. The original image is shown in Figure 2(a). Figure 2(b) and 2(d) compare the performance of the ZA-LMS algorithm obtained by setting $Q = 1$, and the SBR-LMS algorithm with block size $Q = 21$. The step size μ was set to 0.04 for the ZA-LMS, and to 0.01 for the SBR-LMS. We observed that increasing the block size resulted in a faster convergence rate. Thus, to ensure algorithm stability, the step size μ should be small when Q is large. The image restored with ZA-LMS in Figure 2(b) has lower noise level than the original image but deblurring effect is limited. Better results were obtained when we increased the block size as shown in Figure 2(d). The effects of the regularization parameters ρ_s , ρ_t , ρ_z are shown in Figures 2(d)–2(f). All these deconvolution results were obtained with $Q = 21$ and $\mu = 0.01$. They show an increase in resolution compared to the result obtained without regularization in Figure 2(c), where some oscillations can be observed. Smaller values for μ may inhibit this oscillation but may slow down the convergence rate and thus degrade the deblurring efficiency. Besides, the spatial and time piecewise constant penalties controlled by ρ_s and ρ_t led to an improved performance as shown in Figures 2(d) and 2(f). In particular, the oscillations at object edges are reduced. Adding a zero-attracting regularization forces the pixel intensities val-

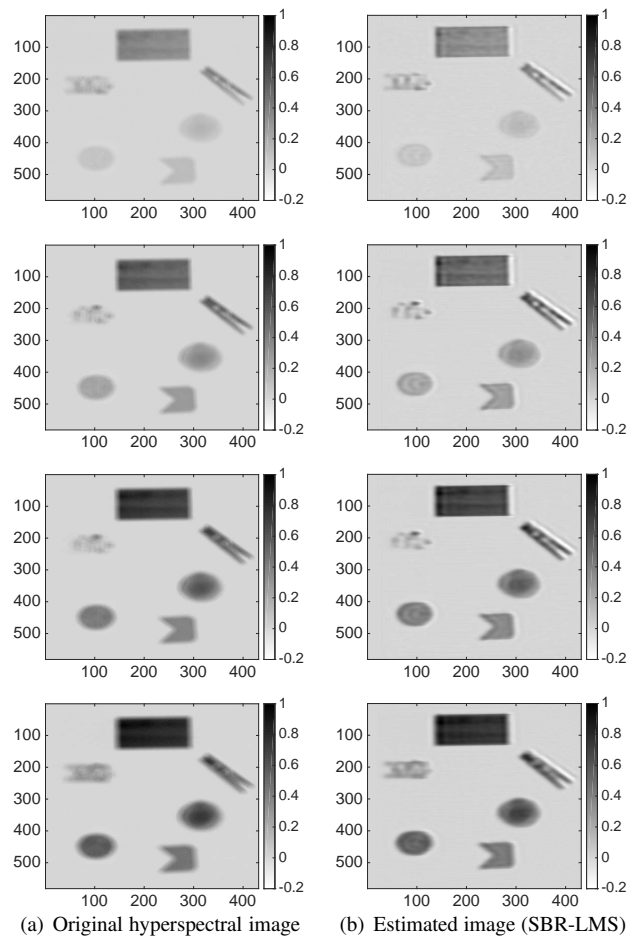


Fig. 3: Hyperspectral image restoration at 4 wavelengths.

ues close to zero to be exactly zero. By comparing Figure 2(e) and 2(f), or Figure 2(c) and 2(d), we conclude that adding the zero-attracting penalty provides better results. Finally, Figure 3 presents the deconvolution result obtained on the whole real hyperspectral image (at 4 wavelengths due to space limitation: 501.1 nm, 623.6 nm, 746.1 nm and 868.6 nm). The coefficients c_p were all set to 1. The original image is shown in Figure 3(a). The image restored with SBR-LMS ($\mu = 0.01$, $Q = 21$, $\rho_s = \rho_t = 3 \cdot 10^{-4}$, $\rho_z = 7 \cdot 10^{-4}$, $\eta_\lambda = 0.001$) is shown in Figure 3(b). The restored images are of better quality from both denoising and deblurring points of view.

5. CONCLUSION

In this work, we addressed the online deconvolution problem of hyperspectral images collected by pushbroom imaging systems. We discussed some issues related to the non-causality of the model. Then, we proposed the SBR-LMS and we evaluated its performance on real hyperspectral data. Future works will be focused on a statistical analysis of the convergence behavior of the SBR-LMS algorithm.

6. REFERENCES

- [1] Jie Chen, Cédric Richard, and Paul Honeine, “Nonlinear unmixing of hyperspectral data based on a linear-mixture/nonlinear-fluctuation model,” *IEEE Transactions on Signal Processing*, vol. 61, no. 2, pp. 480–492, 2013.
- [2] Rita Ammanouil, André Ferrari, Cédric Richard, and David Mary, “Blind and fully constrained unmixing of hyperspectral images,” *IEEE Transactions on Image Processing*, vol. 23, no. 12, pp. 5510–5518, 2014.
- [3] Rebecca M. Willett, Marco F. Duarte, Mark A. Davenport, and Richard G. Baraniuk, “Sparsity and structure in hyperspectral imaging: sensing, reconstruction, and target detection,” *IEEE Signal Processing Magazine*, vol. 31, no. 1, pp. 116–126, 2014.
- [4] Qingli Li, Xiaofu He, Yiting Wang, Hongying Liu, Dongrong Xu, and Fangmin Guo, “Review of spectral imaging technology in biomedical engineering: achievements and challenges,” *Journal of biomedical optics*, vol. 18, no. 10, pp. 100901–100901, 2013.
- [5] Yud R. Chen, Roy W. Huffman, Bosoon Park, and Minh Nguyen, “Transportable spectrophotometer system for on-line classification of poultry carcasses,” *Applied Spectroscopy*, vol. 50, no. 7, pp. 910–916, 1996.
- [6] Hui Huang, Li Liu, and Michael O. Ngadi, “Recent developments in hyperspectral imaging for assessment of food quality and safety,” *Sensors*, vol. 14, no. 4, pp. 7248–7276, 2014.
- [7] Claude Cariou and Kacem Chehdi, “Automatic georeferencing of airborne pushbroom scanner images with missing ancillary data using mutual information,” *IEEE Transactions on Geoscience and Remote Sensing*, vol. 46, no. 5, pp. 1290–1300, 2008.
- [8] Petra Tatzer, Markus Wolf, and Thomas Panner, “Industrial application for inline material sorting using hyperspectral imaging in the NIR range,” *Real-Time Imaging*, vol. 11, no. 2, pp. 99–107, 2005.
- [9] Pellenc Selective Technology, “Mistral product,” <http://www.pellencst.com/products>, Accessed: 2016-09-01.
- [10] Kurt C. Lawrence, Bosoon Park, William R. Windham, and Chengye Mao, “Calibration of a pushbroom hyperspectral imaging system for agricultural inspection,” *Transactions of the ASAE*, vol. 46, no. 2, pp. 513, 2003.
- [11] Brian R. Hunt and Olaf Kubler, “Karhunen-Loeve multispectral image restoration, part I: Theory,” *IEEE Transactions on Acoustics, Speech, and Signal Processing*, vol. 32, no. 3, pp. 592–600, 1984.
- [12] Nikolas P. Galatsanos, Aggelos K. Katsaggelos, Roland T. Chin, and Allen D. Hillery, “Digital restoration of multichannel images,” *IEEE Transactions on Acoustics, Speech, and Signal Processing*, vol. 37, no. 3, pp. 415–421, 1989.
- [13] Nikolas P. Galatsanos, Aggelos K. Katsaggelos, Roland T. Chin, and Allen D. Hillery, “Least squares restoration of multichannel images,” *IEEE Transactions on Signal Processing*, vol. 39, no. 10, pp. 2222–2236, 1991.
- [14] Jean F. Giovannelli and Alain Coulais, “Positive deconvolution for superimposed extended source and point sources,” *Astronomy & Astrophysics*, vol. 439, no. 1, pp. 401–412, 2005.
- [15] Simon Henrot, Charles Soussen, and David Brie, “Fast positive deconvolution of hyperspectral images,” *IEEE Transactions on Image Processing*, vol. 22, no. 2, pp. 828–833, 2013.
- [16] Xile Zhao, Fan Wang, Tingzhu Huang, Michael K. Ng, and Robert J. Plemmons, “Deblurring and sparse unmixing for hyperspectral images,” *IEEE Transactions on Geoscience and Remote Sensing*, vol. 51, no. 7, pp. 4045–4058, 2013.
- [17] Bernard Widrow and Samuel D. Stearns, *Adaptive signal processing*, Englewood Cliffs, NJ, Prentice-Hall, Inc., 1985.
- [18] Yilun Chen, Yuantao Gu, and Alfred O. Hero, “Regularized least-mean-square algorithms,” *arXiv preprint arXiv:1012.5066*, 2010.
- [19] Jie Chen, Cédric Richard, José-Carlos M. Bermudez, and Paul Honeine, “Nonnegative least-mean-square algorithm,” *IEEE Transactions on Signal Processing*, vol. 59, no. 11, pp. 5225–5235, 2011.
- [20] Michael Elad and Arie Feuer, “Superresolution restoration of an image sequence: adaptive filtering approach,” *IEEE Transactions on Image Processing*, vol. 8, no. 3, pp. 387–395, 1999.
- [21] Guilherme H. Costa and José-Carlos M. Bermudez, “Statistical analysis of the LMS algorithm applied to super-resolution image reconstruction,” *IEEE Transactions on Signal Processing*, vol. 55, no. 5, pp. 2084–2095, May 2007.